

Zonda is a novel early component of the autophagy pathway in *Drosophila*

Mariana Melani^{a,b,†}, Ayelén Valko^{a,†}, Nuria M. Romero^{a,†,‡}, Milton O. Aguilera^c, Julieta M. Acevedo^{a,§}, Zambarlal Bhujabal^d, Joel Perez-Perri^{a,||}, Rocío V. de la Riva-Carrasco^a, Maximiliano J. Katz^a, Eleonora Sorianello^{a,b}, Cecilia D'Alessio^{a,b,e}, Gabor Juhász^{f,g}, Terje Johansen^d, María I. Colombo^{b,c}, and Pablo Wappner^{a,b,e,*}

^aFundación Instituto Leloir, Buenos Aires 1405, Argentina; ^bConsejo Nacional de Investigaciones Científicas y Tecnológicas (CONICET), Buenos Aires, Argentina; ^cLaboratorio de Biología Celular y Molecular–Instituto de Histología y Embriología, Facultad de Ciencias Médicas, Universidad Nacional de Cuyo, 5500 Mendoza, Argentina; ^dMolecular Cancer Research Group, Department of Medical Biology, University of Tromsø—The Arctic University of Norway, 9037 Tromsø, Norway; ^eDepartamento de Fisiología, Biología Molecular y Celular, Facultad de Ciencias Exactas y Naturales–Universidad de Buenos Aires, 1428 Buenos Aires, Argentina; ^fDepartment of Anatomy, Cell and Developmental Biology, Eötvös Loránd University, 1053 Budapest, Hungary; ^gInstitute of Genetics, Biological Research Centre, 6726 Szeged, Hungary

ABSTRACT Autophagy is an evolutionary conserved process by which eukaryotic cells undergo self-digestion of cytoplasmic components. Here we report that a novel *Drosophila* immunophilin, which we have named Zonda, is critically required for starvation-induced autophagy. We show that Zonda operates at early stages of the process, specifically for Vps34-mediated phosphatidylinositol 3-phosphate (PI3P) deposition. Zonda displays an even distribution under basal conditions and, soon after starvation, nucleates in endoplasmic reticulum-associated foci that colocalize with omegasome markers. Zonda nucleation depends on Atg1, Atg13, and Atg17 but does not require Vps34, Vps15, Atg6, or Atg14. Zonda interacts physically with Atg1 through its kinase domain, as well as with Atg6 and Vps34. We propose that Zonda is an early component of the autophagy cascade necessary for Vps34-dependent PI3P deposition and omegasome formation.

Monitoring Editor

Denise Montell
University of California,
Santa Barbara

Received: Nov 9, 2016

Revised: Aug 24, 2017

Accepted: Sep 5, 2017

INTRODUCTION

Autophagy, one of the main degradative pathways of the cell, begins with the formation of a membranous cistern called phagophore or isolation membrane that buds from a cup-shaped structure associated with the endoplasmic reticulum (ER) called omega-

some (Axe *et al.*, 2008; Matsunaga *et al.*, 2010; Biazik *et al.*, 2015; Karaniasios and Kistakis, 2015). Thereafter, the phagophore expands and finally seals, giving rise to a double membrane organelle named autophagosome where cytoplasmic components including protein aggregates, ribosomes, and mitochondria are sequestered (reviewed by Mizushima *et al.*, 2008). Soon afterward, autophagosomes acquire degradative enzymes by successive fusion with late endosomes and lysosomes, thereby becoming an autophagolysosome where the engulfed material is degraded (for a revision, see Eskelinen, 2005).

Autophagy, whose main stimulus is the stress generated by nutrient deprivation, is modulated by intracellular signaling pathways, mainly the target of rapamycin (TOR) and AMP-activated protein kinase (AMPK) cascades, as well as by extracellular factors including hormones (e.g., insulin and glucagon) or cytokines (e.g., gamma interferon) (Mizushima *et al.*, 2008). Activation of the ULK1 complex (Atg1 complex in yeast and *Drosophila*) has been described as the first event in the autophagy cascade. This complex, formed by ULK1/2, FIP200/Atg17, Atg13, and Atg101, is constitutively assembled (Hara and Mizushima, 2009), and its kinase activity is negatively

This article was published online ahead of print in MBoC in Press (<http://www.molbiolcell.org/cgi/doi/10.1091/mbc.E16-11-0767>) on September 13, 2017.

[†]These authors contributed equally to this work.

Present addresses: [†]University of Nice-Sophia Antipolis, Institute of Biology Valrose, 06108 Nice, France; [§]German Cancer Research Center, 69120 Heidelberg, Germany; ^{||}European Molecular Biology Laboratory, 69117 Heidelberg, Germany.

*Address correspondence to: Pablo Wappner (pwappner@leloir.org.ar).

Abbreviations used: ATG, autophagy-related; BECN, Beclin; ER, endoplasmic reticulum; FKBP, FK506-binding protein; PI3P, phosphatidylinositol 3-phosphate; TOR, target of rapamycin; ULK, unc-51 like autophagy; VPS, vacuole protein sorting; Zda, Zonda.

© 2017 Melani, Valko, Romero, *et al.* This article is distributed by The American Society for Cell Biology under license from the author(s). Two months after publication it is available to the public under an Attribution–Noncommercial–Share Alike 3.0 Unported Creative Commons License (<http://creativecommons.org/licenses/by-nc-sa/3.0>).

“ASCB®,” “The American Society for Cell Biology®,” and “Molecular Biology of the Cell®” are registered trademarks of The American Society for Cell Biology.

regulated by TOR signaling, which in turn depends on amino acid availability and the energy status of the cell (Anding and Baehrecke, 2015). ULK1/Atg1 regulates the recruitment and activation of a second complex: the Vps34 lipid kinase complex, also called the autophagy nucleation complex, which is composed of the class 3 phosphatidylinositol 3-kinase Vps34 and the proteins PI3KR4 (Vps15), Beclin1 (BECN1)/Atg6, and Atg14 (Juhász *et al.*, 2008; Simonsen and Tooze, 2009; Itakura and Mizushima, 2010; Anding and Baehrecke, 2015; Sanchez-Wandelmer *et al.*, 2015).

Vps34 mediates the synthesis of phosphatidylinositol 3-phosphate (PI3P) (Sanchez-Wandelmer *et al.*, 2015). Local synthesis of this lipid defines the location of omegasome formation and, therefore the site of recruitment of several FYVE domain-containing proteins including DFCP1 and WIPI1, which in turn mediate phagophore elongation and autophagosome formation (Axe *et al.*, 2008; Proikas-Cezanne *et al.*, 2015). Within the Vps34 complex, BECN1 is a direct target of ULK1/Atg1 (Russell *et al.*, 2013), and Vps34 kinase activity is believed to depend on the differential interaction of BECN1 with AMBRA1 or with the anti-apoptotic protein BCL-2 (Gu *et al.*, 2014). BCL-2 binding modulates the levels of BECN1 that become available to interact with Vps34 in the autophagy nucleation complex, thereby contributing to define if the cell will enter apoptosis or activate autophagy (Marquez and Xu, 2012).

FK506-binding proteins (FKBPs) play a role in immunoregulation and participate in critical cellular functions that include protein trafficking and folding. Members of this family display peptidyl prolyl *cis/trans* isomerase (PPIase) activity, participating in *de novo* protein folding through the interconversion of intermediate folding states into the final tridimensional structure (Kang *et al.*, 2008). We have investigated a novel *Drosophila* gene—which we have named Zonda (Zda)—that encodes an immunophilin of the FKBP family, presumably homologous to mammalian FKBP8/FKBP38 (Bhujabal *et al.*, 2017).

By utilizing an *in vivo* approach, we found that Zda is critically required for starvation-induced autophagy. Zda protein displays a cytoplasmic distribution in well-fed larvae and, shortly after the onset of starvation, nucleates in foci that colocalize with omegasome markers. Genetic manipulations revealed that components of the induction complex, Atg1, Atg13, and Atg17, but not components of the Vps34 complex, Vps34, Vps15, Atg6, or Atg14, are required for starvation-induced Zda nucleation. Moreover, Zda interacts physically with Atg1, Atg6, and Vps34 and is necessary for autophagic activation of Vps34 and omegasome formation, as revealed by DFCP1 foci formation following starvation. Zonda overexpression is sufficient to trigger a bona fide autophagic response, as evaluated by different autophagic markers. We propose that Zda is a novel component of the *Drosophila* autophagy machinery that forms part of the omegasome and is required for deposition of PI3P by the Vps34 complex and, hence, for the initiation of autophagosome biogenesis.

RESULTS

Zonda is required for starvation-induced autophagy

We investigated the function of the *Drosophila melanogaster* CG5482 gene product, a presumptive immunophilin of the FKBP family. The predicted protein structure of Zda includes three tetratricopeptide repeat motifs, a calmodulin binding domain, and a transmembrane domain on the C-terminus (Supplemental Figure S1A), the latter being a unique feature within the *Drosophila* FKBP family (Shirane and Nakayama, 2003; Barth *et al.*, 2009). To begin investigating the biology of this gene, which we have called Zonda (Zda), after the name of a wind that blows at the Andes mountain chain, we analyzed its expression by quantitative real-time (RT) PCR and found that it was expressed in all third instar larval tissues, although

at higher levels in the gut and fat body (Supplemental Figure S1B). As a next step, we sought to assess Zda subcellular distribution, for which we generated a mCherry-Zda fusion protein (mCh-Zda), which we expressed in fat body cells of transgenic larvae. In feeding third instar larvae, mCh-Zda was distributed throughout the cytoplasm (Figure 1A). After 6 h of starvation, Zda distribution shifted to a punctate pattern (Figure 1B), suggesting that it might participate in the autophagy process. To investigate this possibility, we performed colocalization experiments with Atg8, a protein that is cytoplasmic in fed conditions and incorporates in autophagic structures on starvation. We utilized a transgenic line expressing GFP-Atg8, in which the green fluorescence displayed ubiquitous distribution in fat body cells of feeding larvae (Figure 1A') and a punctate pattern when the larvae were subjected to starvation (Figure 1B'). Note that 81% of the GFP-Atg8 foci colocalized with mChZda in these starving larvae (Figure 1B''), suggesting that Zda was recruited to autophagic structures. In spite of displaying this dramatic redistribution depending on the feeding status, Zda mRNA is expressed at similar levels in fed or starved individuals (Supplemental Figure S1C).

To analyze whether Zda is necessary for autophagy, we knocked down *zda* by RNA interference (RNAi) expression (*zda*^{RNAi}) in fat body cells (Supplemental Figure S1D) and analyzed the effect on the occurrence of autophagic structures by transmission electron microscopy (TEM). The areas occupied by autophagic structures (Figure 1, C–E) and acidic organelles (Supplemental Figure S1, E–G) in larval fat body cells were remarkably reduced in *zda*^{RNAi} larvae as compared with control individuals expressing an unrelated RNAi (*white* RNAi; *w*^{RNAi}), suggesting that Zda participates in the autophagy process. To confirm this, we analyzed several different autophagy markers in larvae expressing *zda*^{RNAi} in comparison to control *w*^{RNAi} larvae. The behavior of all the tested markers indicated that Zda is indeed required for autophagy (Figure 1, F–Y): First, nucleation of GFP-Atg8 in fat body cells of starving larvae was abolished in *zda*^{RNAi} individuals (Figure 1, F–H and J), and notably, the extent of nucleation inhibition was comparable to that observed after silencing Atg1 (*atg1*^{RNAi}), a key serine/threonine kinase whose activation triggers the autophagy cascade (Figure 1, F, G, I, and J). Interestingly, the Zda requirement for starvation-induced autophagy is not exclusive of fat body cells, as silencing of Zda in salivary glands also prevented nucleation of Atg8 in starved third instar larvae (Supplemental Figure S1, H–J).

As a second criterion, we analyzed the incorporation of LysoTracker, a dye that stains acidic vesicles such as lysosomes and autolysosomes. The LysoTracker pattern changes dramatically in cells that have induced autophagy (Scott *et al.*, 2004), due to the increase in size and number of acidic structures (Saftig and Klumperman, 2009). Whereas LysoTracker staining was faint in fat body cells of feeding larvae of the control genotype (*w*^{RNAi}) (Figure 1K), after 4 h of starvation the LysoTracker signal became stronger and punctate, due to an increase in the size and number of lysosomes (Figure 1L). In fat body cells of starving *zda*^{RNAi} larvae, the LysoTracker pattern was largely abolished (Figure 1, M and O), further indicating that Zda participates in starvation-induced autophagy. Once again, the inhibition provoked by *zda*^{RNAi} was similar to that observed after RNAi-mediated silencing of Atg1 (Figure 1, M–O).

We generated a mutant allele of *zda* by imprecise excision of a P-element inserted 58 base pairs upstream of the 5' end of the gene. The resulting excision removed 1100 base pairs of the coding region, including the transcription initiation site (Supplemental Figure S1K). This resulted in the generation of a *zda* null allele (*zda*^{null}), as confirmed by RT-PCR analysis of *zda* transcript levels in *zda*^{null} homozygous embryos (Supplemental Figure S1L). *zda*^{null} homozygous individuals died at the first larval molt, and viability was

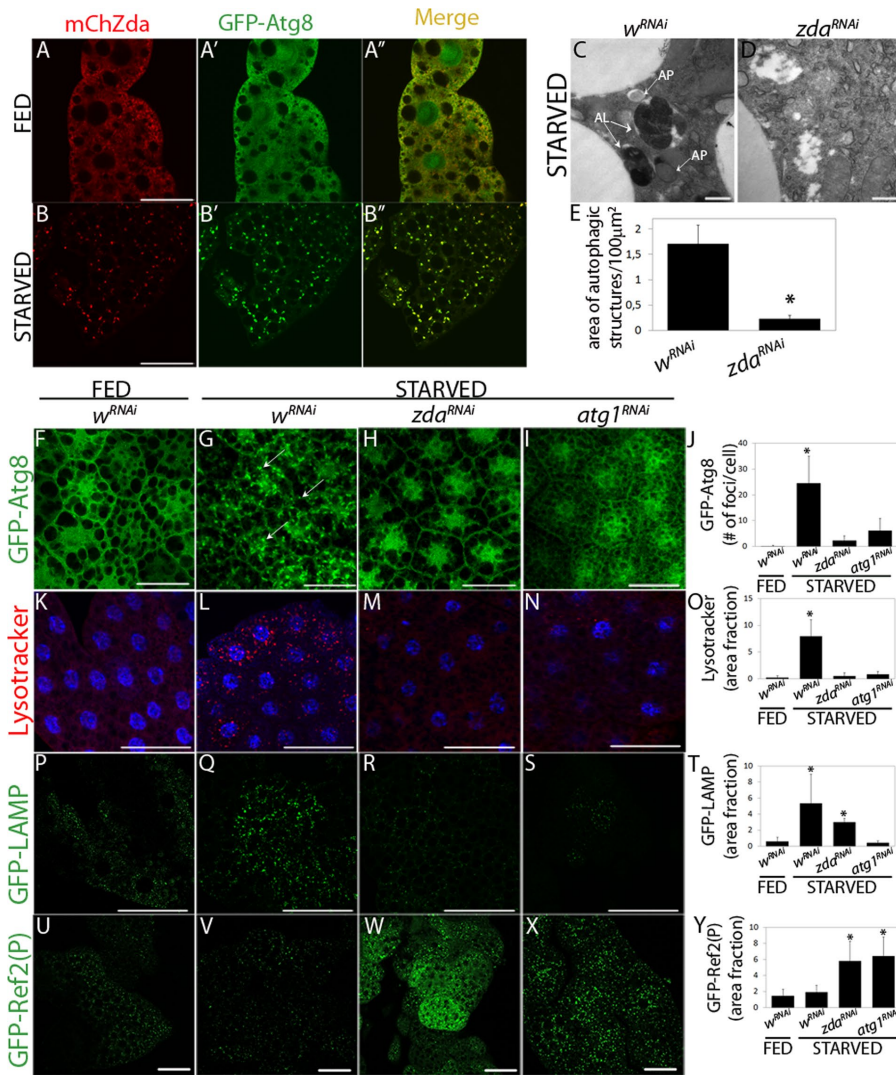


FIGURE 1: Zonda redistributes on starvation and is required for starvation-induced autophagy. (A, B) Zda subcellular localization was sensitive to starvation. Confocal images of fat body cells from fed (A) or starved (B) third instar larvae expressing UAS-mCherry-Zda (mCh-Zda) and UAS-GFP-Atg8 with a *Ppl*-Gal4 driver. In well-fed larvae, GFP-Atg8 and mCh-Zda distributed throughout the cytoplasm. In starved larvae, both proteins colocalized in autophagic structures. (C–Y) Zda is required for starvation-induced autophagy. Transmission electron microscopy images of fat body cells of starved third instar larvae expressing *w^{RNAi}* (C) or *zda^{RNAi}* (D). In control cells autophagic structures, such as autophagosomes (AP) and autolysosomes (AL), could be observed at high frequency, while their occurrence was largely reduced in cells of *zda^{RNAi}* larvae (E), *N* = 3. One-tailed, unpaired Student's *t* test, *p* < 0.05. Scale bar 1 μ m. Confocal images of fat body cells of feeding or starved third instar larvae expressing GFP-Atg8 and the indicated double-stranded RNAs (F–J). GFP-Atg8 was distributed homogeneously in feeding larvae (F) and nucleated in larvae expressing a control RNAi (*w^{RNAi}*) subjected to 4 h starvation (G). This nucleation was prevented in larvae expressing *zda* (H) or *atg1* (I) RNAi. Quantification of GFP-Atg8 puncta is depicted (J), *N* = 40. In control individuals, LysoTracker staining increased sharply 4 h after starvation, revealing the accumulation of lysosomes and autolysosomes (K and L). This increase was blocked in larvae expressing *zda* (M) or *atg1* (N) RNAi. Quantification of the cell area fraction positive for LysoTracker in K–N is shown (O), *N* = 20. In control larvae, GFP-LAMP puncta increased sharply after 4 h starvation, showing once again that lysosomes or autolysosomes accumulated (P and Q). Expression of *zda* (R) or *atg1* (S) RNAi blocked this accumulation, *N* = 20. Quantification of the cell area fraction covered by GFP-LAMP in P–S is depicted (T). A GFP fusion to the adaptor protein Ref(2)P did not accumulate in control larvae in feeding or in starved conditions, indicating that the autophagic flux was normal (U and V). In larvae expressing *zda* (W) or *atg1* (X) RNAi, the autophagic flux was stalled, as indicated by the accumulation of GFP-Ref(2)P. Cell area fraction covered by GFP-Ref(2)P in U–X is depicted (Y), *N* = 20. Data represent mean \pm SD. Means with asterisks are significantly different from *w^{RNAi}* fed. One-way ANOVA followed by a Tukey's test with a confidence interval higher than 95% (*p* 0.05). Scale bar: 50 μ m.

rescued by expression of the *zda* cDNA with *pumpless* or *heat shock*-Gal4 drivers, indicating that the excision generated a bona fide *zda* mutant allele. To confirm the results obtained with *zda^{RNAi}*-mediated silencing, we generated *zda^{null}* homozygous clones by heat shock-induced mitotic recombination (Perrimon and Gans, 1983). Mosaic third instar larvae were subjected to starvation, and LysoTracker incorporation was analyzed in the fat body as well as in wing imaginal discs. Whereas in *zda⁺* cells LysoTracker staining was strong, in *zda^{null}* clones the signal was much weaker (Supplemental Figure S1, M–N). These observations validate the results obtained with the expression of *zda^{RNAi}* and suggest that Zda function in autophagy is cell autonomous.

To continue the characterization of Zda function in autophagy, we analyzed the behavior of two additional autophagy markers, namely Lamp and Ref(2)P. Lamp, which can be visualized through a GFP-Lamp fusion construct, is a lysosomal transmembrane glycosylated protein (Pulipparacharuvi et al., 2005). Whereas in well-fed control larvae, GFP-Lamp displayed a punctate pattern composed of small dots (Figure 1P), this pattern changed to bigger and more abundant GFP-Lamp puncta after starvation (Figure 1, Q and T), indicating that autophagy was activated. Notably, expression of the *zda^{RNAi}* transgene abrogated the accumulation of big GFP-Lamp puncta (Figure 1, R and T) in a comparable manner to that observed following *Atg1* silencing (Figure 1, S and T), further indicating that Zda is necessary for autophagy. Finally, as a fourth marker, we analyzed the accumulation of GFP-Ref(2)P. Ref(2)P is the fly orthologue of mammalian SQSTM1/p62, an adaptor protein normally used to follow the autophagic degradation of ubiquitinated proteins (Bjorkoy et al., 2005). p62/Ref(2)P is degraded at the autolysosome along with ubiquitinated substrates during the autophagy process, and therefore, accumulation of p62/Ref(2)P is a hallmark of impaired autophagic flux. As shown in Figure 1, U, V, and Y, in control larvae GFP-Ref(2)P accumulated minimally in fat body cells of either feeding or starved individuals, which is indicative of an active autophagy flux (Lindmo et al., 2008; Chang and Neufeld, 2009). In contrast, in starved larvae expressing *zda^{RNAi}* or *atg1^{RNAi}* the GFP-Ref(2)P signal increased sharply (Figure 1, W–Y), indicating that autophagic degradation was impaired (Chang and Neufeld, 2009). Altogether the above results show that Zda is necessary for starvation-induced autophagy in *Drosophila* larvae.

Zonda nucleation depends on the Atg1 complex but not on the Vps34 complex

To identify the specific step of the autophagy cascade in which starvation-induced Zda nucleation takes place, we analyzed whether nucleation still occurs after knocking down components of the induction complex, namely Atg1, Atg13, or Atg17. As shown in Figure 2, A–E, silencing of any of the three genes of the induction complex prevented nucleation of mCh-Zda in fat body cells of starving larvae. Nucleation of GFP-Atg8 was used as a positive control, and, as expected, its nucleation also diminished after knocking down Atg1, Atg13, or Atg17 (Figure 2, F–J). Following the same rationale, we analyzed whether elements of the nucleation complex are necessary for Zda foci formation. Neither in larvae expressing a dominant negative form of Vps34 (*vps34^{KD}*) (Juhasz et al., 2008), nor in a line that expressed an RNAi against the same kinase (*Vps34^{RNAi}*) mCh-Zda nucleation was affected (Figure 2, K–M and Q), while nucleation of GFP-Atg8 was largely abolished (Figure 2, R–T and Y). Similar results were observed after silencing additional components of the nucleation complex, namely Vps15, Atg6, or Atg14; none of them affected Zda nucleation (Figure 2, K and N–Q) but prevented formation of GFP-Atg8 puncta (Figure 2, R and U–Y). Taken together, the above results suggest that starvation-induced Zda nucleation depends on the induction complex and is independent of the Vps34 complex.

Zonda is required for Vps34 autophagic function

The above set of results suggests that Zda operates upstream of the Vps34 complex and therefore, that it might be required for Vps34 autophagic activation. Vps34 activity (i.e., deposition of PI3P on

internal cell membranes) can be visualized using PI3P probes such as the GFP-2xFYVE reporter. Vps34 plays a central role at early steps of autophagy but is also required more broadly for several vesicular trafficking processes (Matsunaga et al., 2010). In fat body cells of feeding larvae, GFP-2xFYVE labels early endosomes found around the nuclei, as well as autophagosomes, which are usually more peripheral (Figure 3, A and C) (Juhasz et al., 2008; Matsunaga et al., 2010; Shrivastava et al., 2013). On starvation, a significant increase of peripheral puncta (autophagosomes) occurs in *white^{RNAi}* control larvae, while the number of perinuclear puncta (early endosomes) remains constant (Figure 3, A–C). To investigate whether Zda is required for autophagic activation of Vps34, we analyzed the behavior of the GFP-2xFYVE reporter in larvae expressing *zda^{RNAi}* in parallel with control genotypes such as *vps34^{KD}*, *atg1^{RNAi}* (positive controls), or *atg5^{RNAi}* (negative control). Interestingly, after Zda silencing, the increase of peripheral GFP-2xFYVE foci on starvation was prevented, while perinuclear foci were not affected (Figure 3, D–F, and Supplemental Figure S2, A–D), suggesting that Zda is required for activation of Vps34 specifically during autophagy. As previously reported, expression of the *vps34^{KD}* construct abrogated both the basal GFP-2xFYVE signal in well-fed larvae, as well as the autophagy-triggered increase of peripheral GFP-2xFYVE signal (Figure 3, G–I, and Supplemental Figure S2, A–D) (Juhasz et al., 2008). Consistent with the above results, accumulation of GFP-Rab5 or GFP-Rab7, which label respectively early and late endosomes (Wucherpennig et al., 2003; Zhang et al., 2007; Juhasz et al., 2008), were not affected in *zda^{RNAi}* larvae (Supplemental Figure S2, E–L). As expected, expression of *atg1^{RNAi}* (positive control) interfered specifically with the increase of peripheral foci (autophagosomes) on

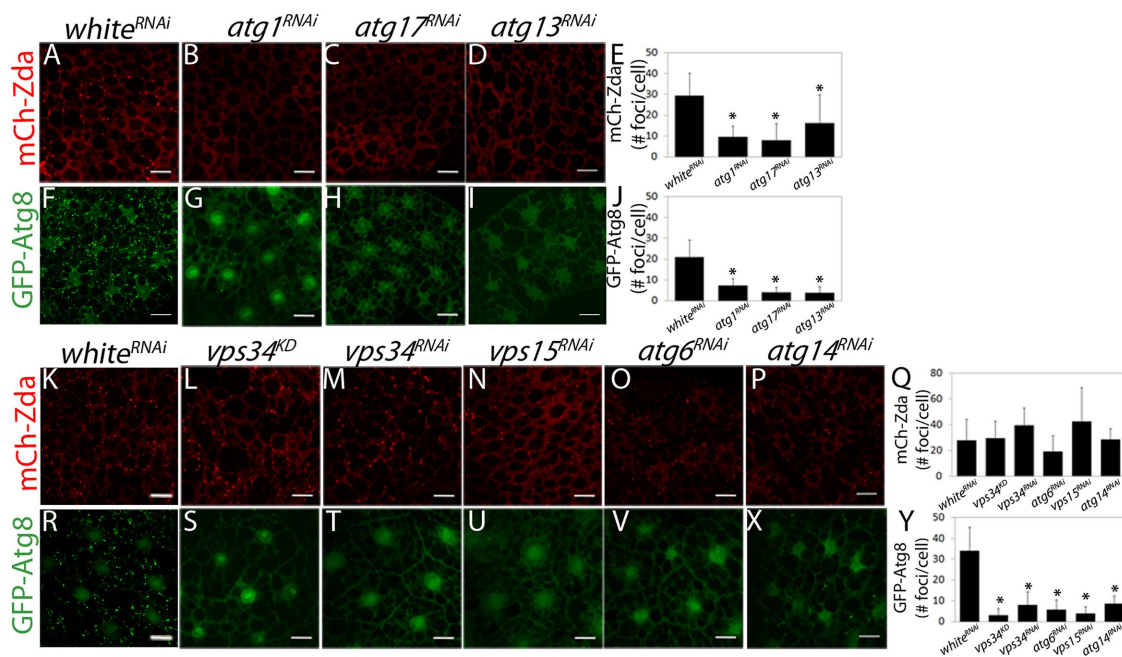


FIGURE 2: Starvation-induced Zda nucleation is downstream of the induction complex and upstream or in parallel of the nucleation complex. Confocal images of fat body cells of starved third instar larvae expressing mChZda (A–D and K–P) or GFP-Atg8 (F–I and R–X) and the indicated RNAi. mCh-Zda (A and K) and GFP-Atg8 (F and R) nucleated in larvae expressing a control RNAi (*w^{RNAi}*). Silencing of the induction complex components *atg1^{RNAi}*, *atg17^{RNAi}*, or *atg13^{RNAi}* blocked starvation-dependent Zda nucleation (B–D) and GFP-Atg8 nucleation (G–I). Inactivation or silencing of the nucleation complex components *vps34^{KD}*, *vps34^{RNAi}*, *vps15^{RNAi}*, *atg6^{RNAi}*, or *atg14^{RNAi}* did not block starvation-induced Zda nucleation (L–P), whereas it did block GFP-Atg8 nucleation (S–X). The mCh-Zda and GFP-Atg8 foci in each condition were counted manually (E, J, Q, and Y). Data represent mean ± SD. Means marked with an asterisk are significantly different. One-way ANOVA followed by a Tukey's test with a confidence interval higher than 99% ($p < 0.01$). Scale bar: 20 μ m. Number of cells counted for each genotype (N): A = 59; B = 87; C = 90; D = 87; F = 67; G = 39; H = 59; I = 40; K = 76; L = 88; M = 85; N = 87; O = 59; P = 77; R = 112; S = 76; T = 84; U = 104; V = 50; X = 69.

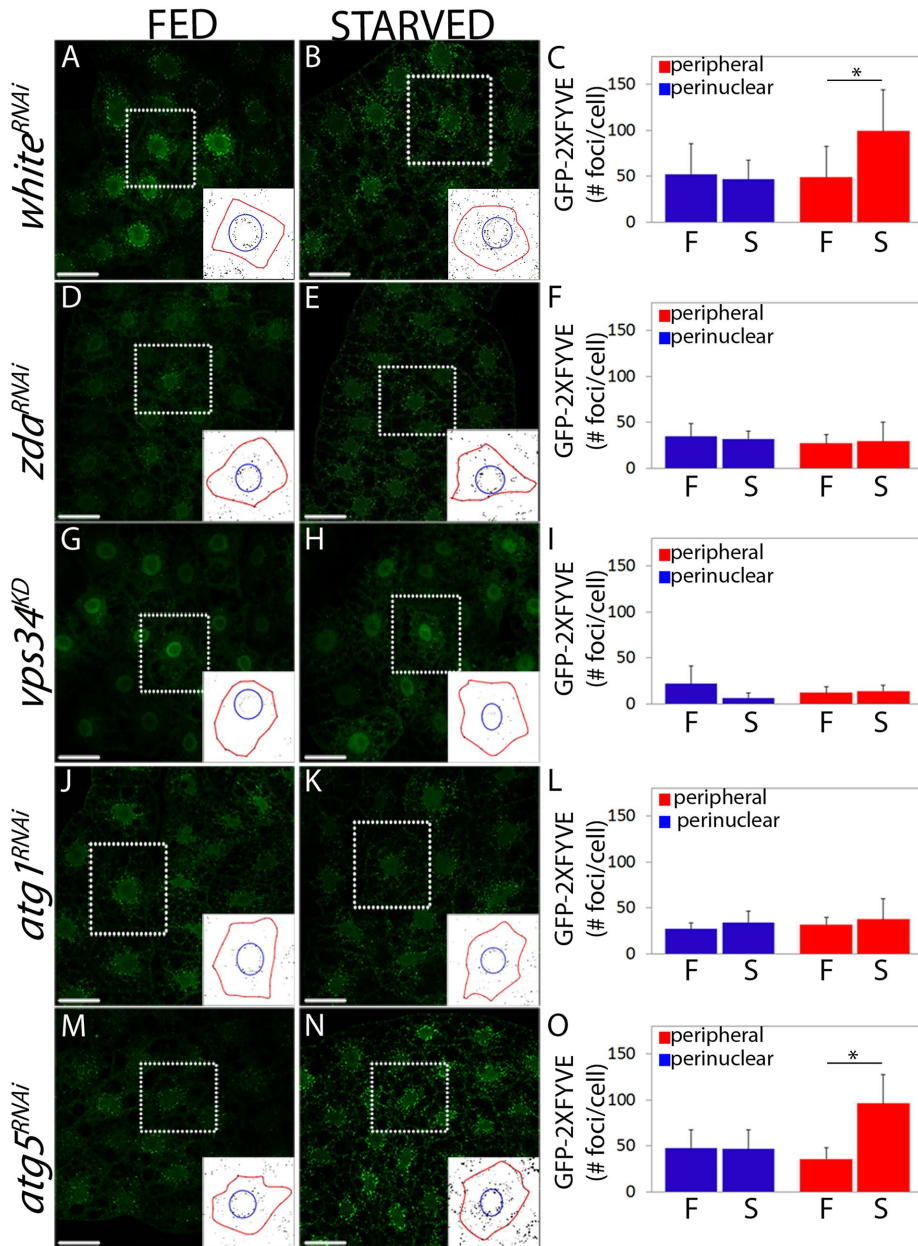


FIGURE 3: Starvation-induced Vps34 activity requires Zda. Confocal images of fat body cells of fed (A, D, G, J, and M) or starved (B, E, H, K, and N) third instar larvae expressing the PI3P reporter GFP-2xFYVE. *white^{RNAi}* (A and B), *zda^{RNAi}* (D and E), *vps34^{KD}* (G and H), *atg1^{RNAi}* (J and K), or *atg5^{RNAi}* (M and N) were coexpressed. In control larvae under feeding conditions, a proportion of the GFP-2xFYVE signal was perinuclear (corresponding to endosomes), while another proportion was more peripheral (autophagosomes) (A). Following starvation, the peripheral signal of the reporter increased significantly, while the perinuclear signal remained constant (B). In larvae expressing *zda^{RNAi}* (D and E) or *atg1^{RNAi}* (J and K) the GFP-2xFYVE signal did not change after starvation, indicating that autophagic activation of Vps34 was blocked. In larvae expressing *atg5^{RNAi}* (M and N), starvation-induced activation of Vps34 was normal. Expression of a dominant negative form of Vps34 (*vps34^{KD}*) largely suppressed the GFP-2xFYVE signal both under feeding (G) or starving (H) conditions. The insets depict how the GFP-2xFYVE signal was quantified in the perinuclear (within the blue circle) and peripheral regions (between the blue circle and the red line that marks the plasma membrane). The reporter signal (number of foci) was quantified in each of these two regions in at least 20 cells of three independent experiments (C, F, I, L, and O). Data represent mean \pm SD. One-tailed, unpaired Student's *t* test, $p < 0.05$. Scale bar: 50 μ m. Number of cells counted for each genotype and condition (N): A = 8; B = 12; D = 12; E = 12; G = 9; H = 9; J = 8; K = 9; M = 9; N = 12.

starvation (Figure 3, J–L), and notably, the extent to which the autophagic activation of Vps34 depends on Zda was similar to its dependence on Atg1 (Figure 3, D–F and J–L). The autophagic increase of GFP-2xFYVE peripheral signal did not depend on Atg5 (negative control), a molecule involved in Atg8 lipidation and therefore known to operate downstream of Vps34 (Figure 3, M–O). Collectively the above set of results indicates that Zda is required for autophagic activation of Vps34 and, hence, for PI3P deposition on locations where formation of the omegasome will take place.

Zonda physically interacts with Atg1, Vps34, and Atg6

Given the above genetic evidence indicating that Zda operates downstream or in parallel to Atg1 and upstream of the Vps34 nucleation complex, we assessed physical interactions of Zda with Atg1 and with elements of the nucleation complex. Using glutathione *S*-transferase (GST) pull-down assays, we found that Zda binds directly to Atg1, and domain analysis revealed that Zda–Atg1 interaction requires the Atg1 kinase domain (Figure 4, A–C). Deletion of this domain (amino acids 10–280; Figure 4A) completely prevented binding to Zda (Figure 4, B and C). Next we assessed whether Zda also interacts with members of the nucleation complex. Indeed, we detected direct physical interaction of Zda with Vps34 (Figure 4D) and with Atg6 (Figure 4E). Altogether these results suggest that Zda directly interacts with Atg1 and with the components of the nucleation complex Vps34 and Atg6.

Zonda is required for omegasome formation and localizes at the omegasome

The omegasome has been described in mammals as a membranous structure that forms in association with the ER from where the phagophore emerges (Axe *et al.*, 2008), so it is considered the earliest distinguishable autophagic structure. We investigated if formation of the omegasome is impaired in *zda^{RNAi}* larvae. The omegasome can be visualized as a ring or omega-shaped structure when labeled with PI3P probes such as FYVE domain constructs fused to fluorescent proteins. Shortly after formation, omegasomes become loaded with the autophagy proteins Atg5 and Atg8 that mark the phagophore, which afterward gives rise to the autophagosome (Axe *et al.*, 2008; Roberts and Ktistakis, 2013). DFCP1 is a

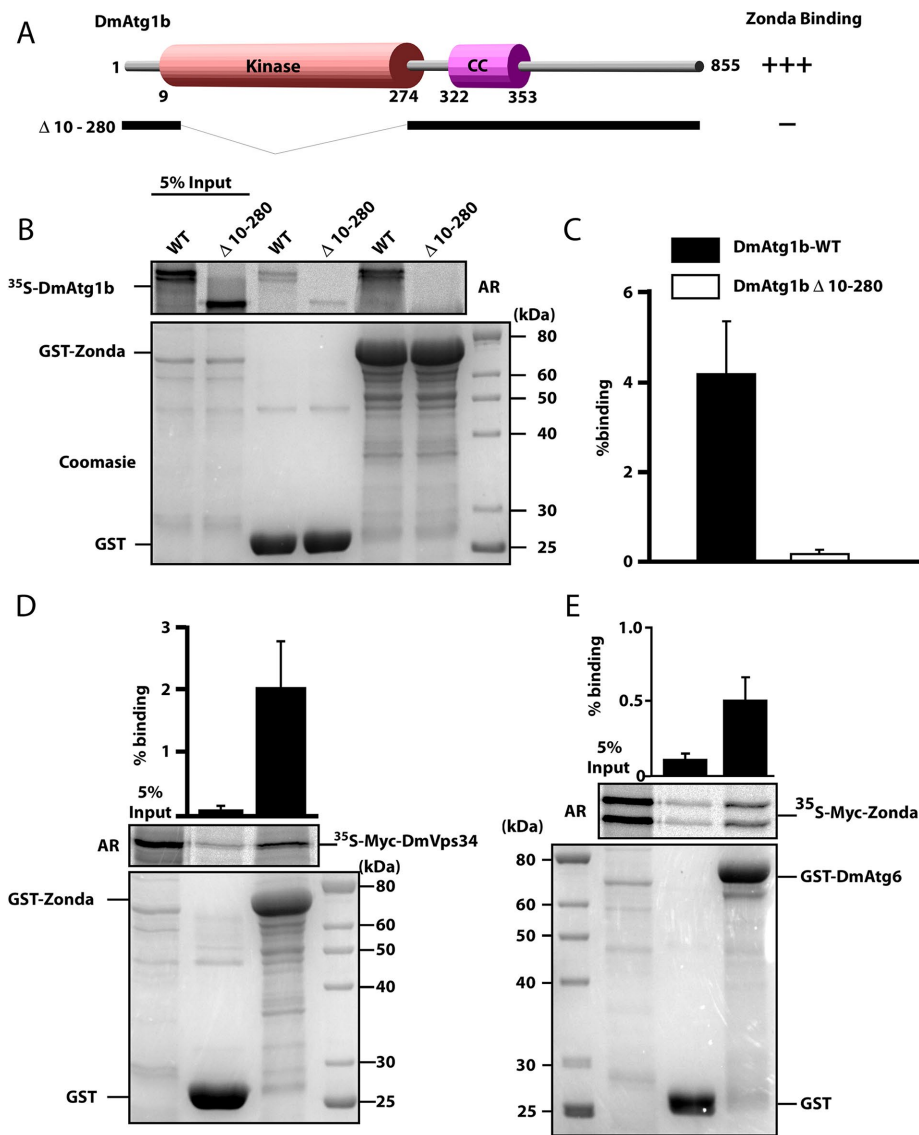


FIGURE 4: Zda binds directly to Atg1B, Atg6, and Vps34 in vitro. (A) Schematic representation of the DmAtg1b domain structure and deletion constructs made to determine domain-mediated binding to Zda. (B) GST pull-down assay using in vitro-translated ^{35}S -labeled Myc-tagged Dm-Atg1B. In vitro-translated full length, or a kinase domain deletion mutant, of Myc-tagged DmAtg1B were incubated with recombinant GST or GST-Zda expressed in *E. coli* attached to glutathione-sepharose beads and bound protein was detected by autoradiography (AR). The Coomassie-stained SDS-PAGE gel indicates the amount of GST protein used in the assay. The graph displays percentage binding of in vitro-translated protein relative to the input. (C) Similar to B except that in vitro-translated ^{35}S -labeled Myc-tagged Zda was incubated with GST or GST-DmAtg6. Quantifications with mean values and SDs from three independent experiments of the binding assays are shown in the graph bar diagram. (D) Similar to B, except that in vitro-translated ^{35}S -labeled Myc-tagged DmVps34 was incubated with GST or GST-Zda. The graph represents the mean value with SD from three independent experiments.

component of mammalian omegasomes and therefore is usually utilized to identify these early autophagy structures (Axe *et al.*, 2008). In an attempt to visualize *Drosophila* omegasomes, and given that a DFCP1 homologue does not exist in *Drosophila*, specific markers for the *Drosophila* omegasome are not currently available, and considering that human DFCP1 expressed in *Caenorhabditis elegans* localizes at the worm omegasome (Lu *et al.*, 2011), we generated a transgenic fly line expressing human DFCP1 fused to GFP on its N-terminus (GFP-DFCP1). As shown in Supplemental Figure S3, the heterologous DFCP1 construct became incorporated into structures

reminiscent of mammalian omegasomes, with a ring shape of 0.7 μm diameter on average, which colocalized with the PI3P reporter myc-2xFYVE (Supplemental Figure S3A and Supplemental Movie S1) (Gillooly *et al.*, 2000). Remarkably, these ring-shaped structures contained a particle of RFP-Atg5 (Supplemental Figure S3B and Supplemental Movie S2) (Barth *et al.*, 2011) or mCh-Atg8 (Supplemental Figure S3C and Supplemental Movie S3) within the ring—presumably the phagophore budding off—as was previously reported for mammalian omegasomes (Axe *et al.*, 2008). We therefore conclude that mammalian GFP-DFCP1 labels the *Drosophila* omegasome.

As expected, in control larvae, the occurrence of GFP-DFCP1 foci increased significantly after starvation (Figure 5, A, B, and E), indicating induction of omegasome biogenesis following the autophagic stimulus. Interestingly, this increase was prevented in *zda^{RNAi}* individuals (Figure 5, A, C, and E), consistent with a role of Zda in omegasome formation. Notably, omegasome formation following starvation was prevented to a similar extent in larvae expressing the Vps34 dominant negative construct (Figure 5, A, D, and E). Taken together, these results suggest that Zda plays a role in biogenesis of the omegasome.

Given that Zda was required for autophagic activation of Vps34 and omegasome formation (Figures 3 and 5), we performed detailed colocalization analysis of mCh-Zda with ER, omegasome, and phagophore markers. Several lines of evidence suggest that Zda localizes at the omegasome: mCh-Zda formed 0.5- to 1.0- μm -diameter rings or omega-like structures. These structures colocalized with the ER marker GFP-PDI (Figure 6, A and F), with the omegasome marker GFP-DFCP1 (Figure 6, B and F, and Supplemental Movie S4), as well as with GFP-2xFYVE rings (Figure 6, C and F, and Supplemental Movie S5). Interestingly, we detected Zda ring-shaped structures containing a particle of GFP-Atg5 (Figure 6, D and F, and Supplemental Movie S6) or GFP-Atg8 (Figure 6, E and F, and Supplemental Movie S7) budding off from the omegasome, which presumably represents the phagophore.

These results suggest that Zda is a novel component of the *Drosophila* omegasome.

It was recently reported that FKBP8/FKBP38, a mammalian membrane immunophilin that is presumably the orthologue of *Drosophila* Zda, participates in mitophagy (Bhujabal *et al.*, 2017). We therefore analyzed if Zda remains associated with late autophagy structures in fat body cells of larvae subjected to starvation and found that this was indeed the case. Colocalization studies with GFP-Atg8 or GFP-Lamp revealed that Zda localizes also at autophagosomes and autolysosomes but not at lysosomes (Figure 7, A–F). Consistent with

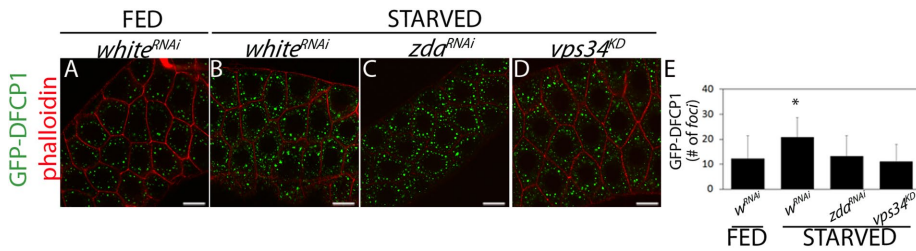


FIGURE 5: Starvation-induced DFCP1 deposition requires Zonda. Confocal images of salivary gland cells of fed (A) or starved (B–D) third instar larvae expressing GFP-DFCP1 (green) and labeled with rhodamine-phalloidin (red). *white*^{RNAi} (A and B), *zda*^{RNAi} (C), or a *vps34*^{KD} (D) were coexpressed. Starvation induced an increase in the number of DFCP1 foci in *white*^{RNAi} larvae, indicating omegasome formation (A and B). Zda silencing (C) or Vps34 activity blockage (D) abolished this increase. The number of GFP-DFCP1 foci per cell was quantified in each condition (E), $N = 40$. Data represent mean \pm SD. Means marked with an asterisk are significantly different. One-way ANOVA followed by a Tukey’s test with a confidence interval higher than 95% ($p < 0.05$). Scale bar: 20 μ m.

the recent study performed in mammalian cells (Bhujabal *et al.*, 2017), we observed at high frequency that the mitochondrial marker Mito-GFP appeared within these late Zda-containing autophagy structures (Figure 7, G–I), suggesting that *Drosophila* Zda might also participate in mitophagy. This set of data suggests that Zda participates in at least two different steps of the autophagy process: First, it is required for omegasome formation and later remains associated with mature autophagy structures.

Overexpression of Zonda triggers autophagy

Having established that Zda is required for autophagy and that it can interact with Atg1, we sought to investigate whether, as is the

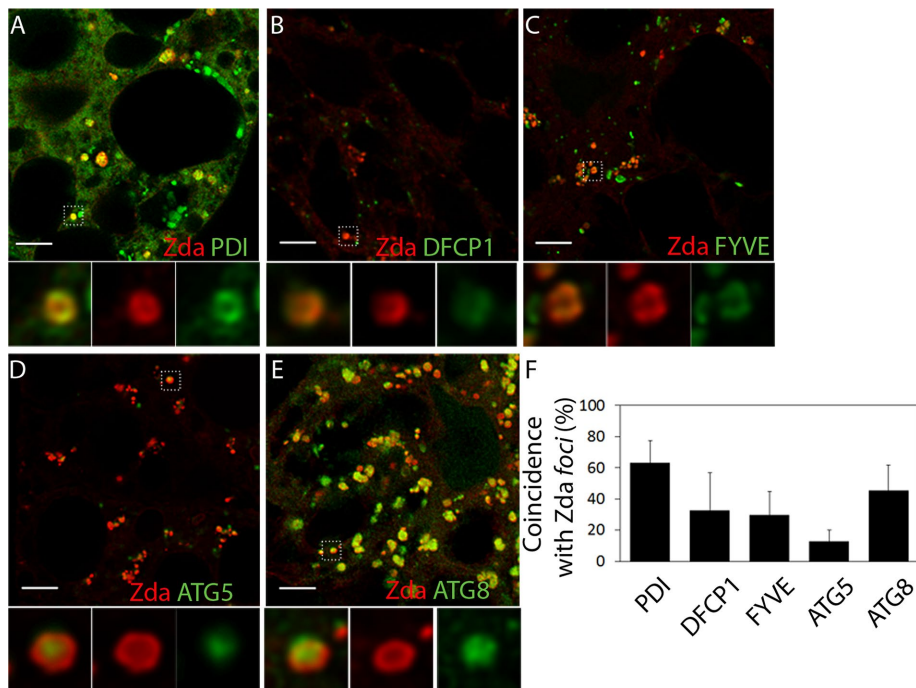


FIGURE 6: Zonda localizes at the omegasome. Confocal images of fat body cells of starving third instar larvae coexpressing mCh-Zda along with GFP-PDI (A), GFP-DFCP1 (B), GFP-2xFYVE (C), GFP-Atg5 (D), or GFP-Atg8 (E). A magnified view of the omegasomes for each panel is shown in the insets. The percentage of colocalization between Zonda foci and each of the markers is shown in F. Zda formed rings on the ER (A–A’) that colocalized with the omegasome markers GFP-DFCP1 (B–B’) and GFP-2xFYVE (C–C’). Phagophore markers GFP-Atg5 (D) and GFP-Atg8 (E) are observed in the center of Zda-containing rings, which are presumably omegasomes. Scale bar: 5 μ m. Number of fields counted for each genotype (N): A = 5; B = 6; C = 7; D = 7; E = 8.

case for Atg1 (Scott *et al.*, 2007), Zda overexpression can trigger autophagy, and to this end we expressed two copies of mCh-Zda at 25°C in well-fed larvae. TEM analysis revealed that Zda overexpression provoked a dramatic accumulation of autophagic structures in fat body cells of third instar larvae (Figure 8, A, C, and D) and, remarkably, this accumulation was comparable to that observed on starvation of wild-type controls (Figure 8, A–D). Then we assessed autophagy induction by GFP-Atg8 nucleation and LysoTracker staining. Both criteria confirmed autophagy induction (Figure 8, E–G and J, and K–M and P). As a next step, we investigated whether autophagy induction provoked by Zda overexpression was dependent on Atg1 or Vps34, so we over-

expressed Zda in an Atg1 null mutant background or in a strain that coexpressed the Vps34 dominant negative construct. Whereas in the Atg1 mutant background Zda-induced autophagy diminished (Figure 8, E–H and J, and K–N and P), the coexpression of *Vps34*^{KD} totally prevented autophagy induction (Figure 8, E–G, I, and J, and K–M, O, and P). These results indicate that Zda-induced autophagy partially requires Atg1 and depends completely on Vps34.

To continue with the characterization of Zda-induced autophagy, we wondered as whether autophagy flux is normal following Zda overexpression, and we utilized for this an alternative overexpression method in which a single copy of the transgene was expressed at 29°C. This overexpression method was as efficient as the one

utilized above, as revealed by Atg8 nucleation (Supplemental Figure S4, A–D). Interestingly, analysis of the GFP-Ref(2)P reporter demonstrated that the autophagy flux is not stalled (Supplemental Figure S4, E–H), suggesting that autophagy proceeds normally after Zda-dependent induction of the process. We also investigated if Zda overexpression provokes accumulation of omegasomes and found that this was indeed the case, as revealed by increased signal of the omegasome-specific GFP-DFCP1 reporter (Supplemental Figure S4, I–L), as well as by the specific increase of GFP-2xFYVE peripheral puncta (Supplemental Figure S4, M–P). Collectively this set of results indicates that sufficient levels of Zda protein are enough to induce a bona fide autophagy process even in conditions of nutrient abundance, strengthening the notion that Zda operates at early phases of the autophagy cascade.

Zda is a negative regulator of growth and inhibits the TOR pathway

Previous studies in *Drosophila* larvae demonstrated that Atg1 negatively regulates the TOR pathway, leading to reduction of cell growth (Lee *et al.*, 2007; Scott *et al.*, 2007). Given that Zonda is an early component of the autophagy cascade, we sought to investigate its effect on tissue and cell growth. First, we generated *zda*^{null} *eyeless* FLP-FRT

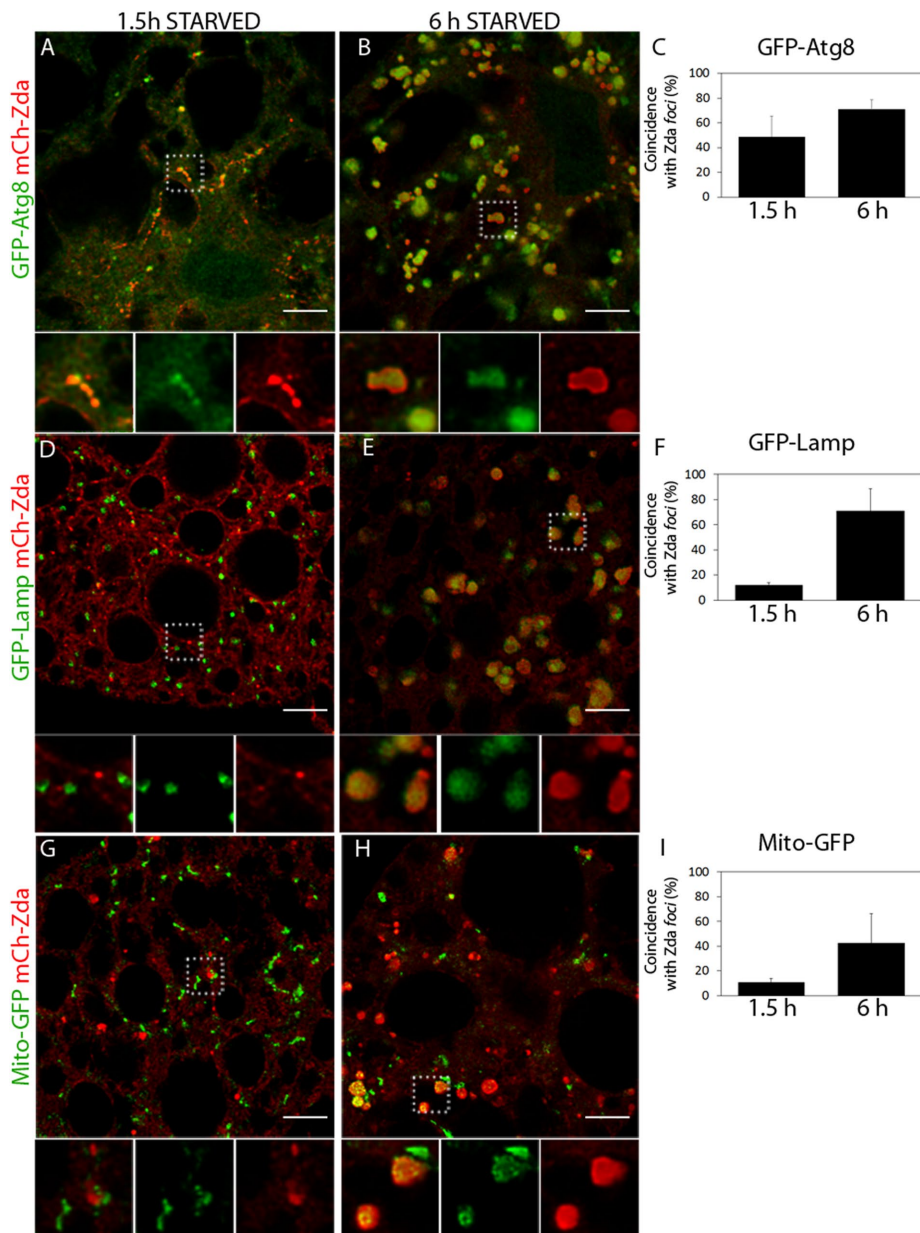


FIGURE 7: Zonda localizes at autophagosomes and autolysosomes. Confocal images of fat body cells of starving third instar larvae coexpressing mCh-Zda along with GFP-Atg8 (A and B), GFP-Lamp (D and E), and Mito-GFP (G and H). A magnified view of the structures for each panel is shown in the insets. The percentage of colocalization between Zonda foci and each of the markers is shown in C, F, and I. Zda and Atg8 are part of the same structure at both early and late starvation times. Zonda does not colocalize with GFP-Lamp nor with Mito-GFP-labeled structures at early starvation times, but it does colocalize with these markers at later starvation periods, which indicates that Zonda is not present at lysosomes or mitochondria but is present at autophagosomes and autolysosomes. Scale bar: 10 μ m. Number of fields counted for each genotype (N): A = 8; B = 6; D = 4; E = 4; G = 4; H = 5.

(Flippase-Flippase Recognition Target) clones (Newsome *et al.*, 2000) and observed significant increase of head size (Figure 9, A–C), while thorax size was unaffected. Next we overexpressed Zda in FLP-out clones and observed in the fat body that increased levels of Zda provoked cell size reduction (Figure 9, D and E). These results indicate that Zda is a negative regulator of growth. As a next step, we investigated if Zda can modulate the TOR pathway, so we performed Western blot analysis of phosphorylated S6 kinase (pS6K), a hallmark of TOR pathway activation (Laplante and Sabatini, 2009).

As depicted in Figure 9F, pS6K was clearly reduced in larvae that overexpressed Zda. Collectively these results suggest that Zda contributes to restrict cell and organ growth through the inhibition of the TOR pathway.

DISCUSSION

In this work, we describe a previously uncharacterized *Drosophila* immunophilin named Zonda (Zda) that functions as an upstream positive component of the autophagy cascade. Previously, other immunophilins have been proposed both as positive or negative regulators of autophagy. In *Drosophila*, FKBP39 was found to be a negative regulator of developmentally triggered autophagy, possibly through the regulation of the transcription factor Foxo (Juhász *et al.*, 2007). Mammalian FKBP51 was described as a scaffold protein that recruits PHLPP, Akt, and Beclin1, leading to activation of autophagy (Albu *et al.*, 2014). More recently, FKBP38 has been reported as a mitophagy receptor that interacts with LC3. Coexpression of FKBP38 along with LC3 can trigger Parkin-independent mitophagy (Bhujabal *et al.*, 2017).

Based on sequence homology, Zda is the likely orthologue of FKBP38. Not only do they share characteristic domains of FKBP proteins (Kang *et al.*, 2008), but both proteins are the only members of their families to have a transmembrane domain on their C-terminal end. We have shown that Zda is required for starvation-induced autophagy. Larval fat body cells in which Zda expression has been silenced fail to trigger autophagy, as assessed by several independent criteria: 1) inability of the cells to form autophagosomes and autolysosomes after starvation, as assessed by TEM and Atg8 nucleation; 2) their inability to increase the number and size of lysosomes, as evaluated by Lyso-Tracker and GFP-Lamp markers; and 3) accumulation of Ref(2)P in these cells, which is indicative of impaired autophagic flux.

We have found that, after nutrient deprivation, Zda can be detected in omegasomes, colocalizing with PI3P and DFCP1, from which early autophagic structures labeled with GFP-Atg5 and GFP-Atg8 bud off. Consistent with the notion that Zda is an early component of the autophagy cascade,

our genetic analysis revealed that starvation-induced Zda nucleation depends fully on components of the Atg1 induction complex but not on components of the Vps34 nucleation complex. Vps34 autophagic activation following starvation is regulated by the nutritional status of the cell downstream of Atg1 (Juhász *et al.*, 2008). We found that Zda interacts physically with the Atg1 kinase domain, as well as with components of the nucleation complex, including Atg6 and Vps34, suggesting that it may contribute to the activation of the latter complex by Atg1. This notion is consistent with the results of

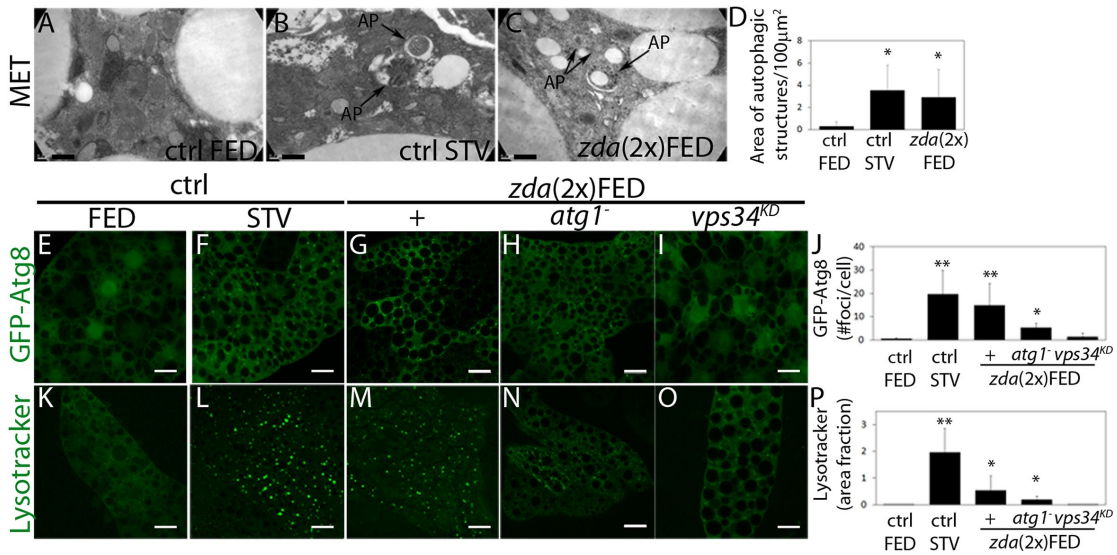


FIGURE 8: Zonda overexpression induces autophagy. (A–C) Transmission electron microscopy images of fat body cells of control animals under feeding (A) or starved (B) conditions or Zonda-overexpressing feeding larvae (C). The area of autophagic structures per 100 μm² was quantified (D), N = 3. Scale bar: 1 μm. (E–I) Confocal images of fat body cells of third instar larvae under feeding (E and G–I) or starved (F) conditions. In all cases, the autophagosome marker GFP-Atg8 was expressed under the control of *ppl-Gal4* driver. (G–I) Panels G–I also express two copies of a mCh-Zda in wild-type (G), *atg1Δ³* (H) or *vps34^{KD}* (I) background. (J) Quantification of the number of GFP-Atg8 foci per cell in each of the indicated genotypes. Overexpression of two copies of mCh-Zda is sufficient to induce GFP-Atg8 nucleation (G). This nucleation depends on *atg1* (H) and *vps34* (I). (K–P) Confocal images of fat body cells of third instar larvae under feeding (K and M–O) or starved (L) conditions. Lysosomal marker (LysoTracker) incorporation was analyzed. (M–O) Panels M–O also express two copies of a mCh-Zda in wild-type (M), *atg1Δ³* (N), or *vps34^{KD}* (O) background. (P) Quantification of the cell area fraction positive for LysoTracker in each of the indicated genotypes. Overexpression of two copies of mCh-Zda is sufficient to induce LysoTracker incorporation (M). This phenotype depends on *atg1* (N) and *vps34* (O). Data represent mean ± SD. Means with different number of asterisks are significantly different. One-way ANOVA followed by a Tukey’s test with a confidence interval higher than 95% (*p* < 0.05). Scale bar: 10 μm. Number of cells counted for each genotype and condition (N): E = 20; F = 21; G = 29; H = 34; I = 20; K = 19; L = 18; M = 28; N = 25; O = 17.

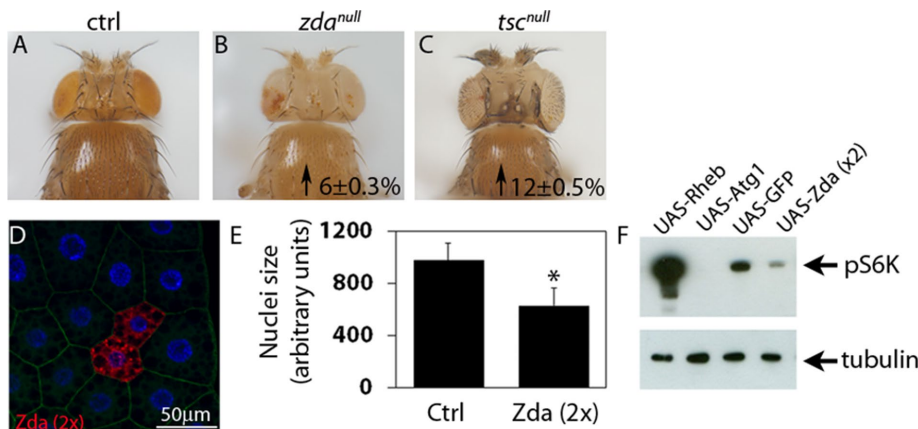


FIGURE 9: Zonda is a negative regulator of Tor. (A–C) Representative heads of the indicated genotypes. Mutant heads were generated using *eyeless*-induced FLP-mediated recombination. Homozygous *wild-type* cells were eliminated due to the presence of a *minute* mutation in the recombined chromosome. In comparison to control heads (*FRT82*, A), *zda^{null}* heads are bigger. As a positive control, *tsc^{null}* heads were generated, and they are also bigger than controls. Numbers inside panels represent the incremental percentage with respect to control heads. The increments are statistically significant, *p* < 0.05. (D) An example of a fat body containing wild-type and mCh-Zda-overexpressing cells is shown in D. DAPI labels cell nuclei. (E) Quantification of nuclei size of control fat body cells or Zonda-overexpressing fat body cells (UAS-Zda 2x). Zonda overexpressing cells were generated using the flip-out technique. N = 20. Two-tailed, unpaired Student’s *t* test, *p* < 0.05. (F) Western blot analysis of larval homogenates overexpressing the indicated UAS constructs using a *ppl-Gal4* driver. Membranes were blotted with antibodies against phospho-S6K and tubulin. A representative membrane from three independent experiments is shown. Number of heads counted for each genotype (N): A = 30; B = 35; C = 28. Number of cells counted (N): D = 20.

our genetic experiments utilizing early autophagy markers, as they suggest that autophagy-dependent Vps34 activation and omegasome formation are dependent on Zda, this dependence being comparable to that on Atg1. Unlike Atg6, which was shown to be also required for Vps34 basal activity (Shrivage et al., 2013), Zda is clearly not necessary for early endosome formation but only for autophagic activation of Vps34. Thus, given the requirement of Zda for Vps34 autophagy-specific activation, and based on its localization at the omegasome, we propose that Zda contributes to define the location on the ER at which Vps34-dependent PI3P deposition and omegasome formation take place (Figure 10).

Induction of autophagy depends on the nutritional status of the cell and is subject to a contra-regulatory mechanism that occurs between mTOR and Atg1 (Chen and Klionsky, 2011). Under nutrient-rich conditions, active mTOR phosphorylates and inactivates the Atg1 complex (Chang and Neufeld, 2009; Kamada et al., 2010; Kishi-Itakura et al., 2014), and when nutrients are scarce, mTOR-dependent inactivation of Atg1 is released. Atg1 in turn reinforces down-regulation of mTOR through mechanisms that

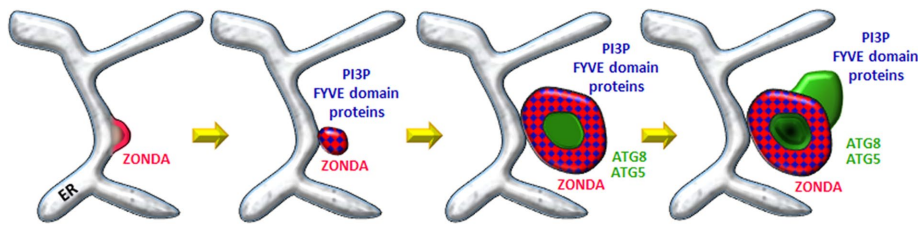


FIGURE 10: Model for the mode of action of Zonda in omegasome formation. From left to right: Shortly after starvation Zda nucleates on the ER and the Zda-labeled sites function as platforms for Vps34-dependent PI3P deposition. ER domains enriched in PI3P evolve into ring-shaped omegasomes from which phagophores containing Atg5 and Atg8 bud off.

remain poorly defined (Chang and Neufeld, 2009). In line with this, *Drosophila* fat body cells that are mutant for *atg1* grow bigger than control cells when subjected to prolonged nutrient deprivation, and conversely, Atg1 overexpression provokes cell size reduction and induces autophagosome formation (Chang and Neufeld, 2009). We have shown here that when overexpressed above certain levels, Zda can trigger a bona fide autophagic process, as assed by several indicators, including TEM, Atg8 nucleation, and LysoTracker incorporation. We have shown that this autophagic response fully depends on the activity of Vps34 and partially on Atg1. This suggests that Zonda operates upstream of Vps34 and in parallel to Atg1. Consistent with this, we observed that under the same overexpression conditions, the TOR pathway is down-regulated and cell size is reduced similarly to what has been reported for Atg1 (Lee *et al.*, 2007; Scott *et al.*, 2007). In line with these observations, adult flies that are homozygous for a Zda null mutation specifically in the head exhibit larger heads. Thus Zda mediates negative regulation of TOR, thereby exerting cell-autonomous negative regulation of growth.

Given that immunophilins are known to work as chaperons or scaffolds (Kang *et al.*, 2008), we propose that Zda might provide a platform where Atg1 and the Vps34 complex interact. Further research is required to define the mechanism by which Zda cooperates with Atg1 on the activation of the Vps34 nucleation complex that culminates in localized PI3P deposition for omegasome formation.

MATERIALS AND METHODS

Fly stocks

Flies were raised at 25°C on standard cornmeal/agar medium. In all experiments, larvae were sorted 24 h after egg deposition. Thirty to 40 larvae were grown per vial for each experimental condition at 25°C or 29°C depending on the experiment. When required, larvae were starved for the indicated periods of time on agar plates. The following *D. melanogaster* lines were from the Bloomington Stock Center (<http://flystocks.bio.indiana.edu>): *w¹¹¹⁸* (BL 3605), *actin-Gal4* (BL 4414), *pumpless-Gal4* (*ppl-Gal4*) (BL58768), *UAS-GFP-2xFYVE* (BL42712), *UAS-GFP-PDI* (BL 6839), *UAS-GFP-Atg5* (BL 50877), *UAS-mito-GFP* (BL 25747), *UAS-GFP-Rab5* (BL 43336), *white^{RNAi}* (BL 33613), *atg17^{RNAi}*(BL36918) *atg14^{RNAi}*(BL40858) *Vps15^{RNAi}*(BL34092), *Vps34^{RNAi}* (BL33384), and *FRT42D*. *zda^{RNAi}* (v110620), *atg1^{RNAi}* (v16133), *atg13^{RNAi}* (v103381), and *atg6^{RNAi}* (v22123) were from the Vienna *Drosophila* RNAi Center (VDRC, <http://stockcenter.vdrc.at>). *UAS-Atg1*, *UAS-GFP-Atg8*, *UAS-mCherry-Atg8*, *UAS-GFP-Ref(2)P*, and *UAS-Vps34^{DN}* were kindly provided by Thomas Neufeld (University of Minnesota, Minneapolis) (Juhasz *et al.*, 2008); *UAS-GFP-LAMP* was provided by Helmut Kramer (University of Texas Southwestern Medical Center, Dallas) (Pulipparacharuvil *et al.*, 2005); *UAS-GFP-Rab7* and *UAS-myc-2xFYVE* were provided by Marcos González-Gaitán (University of Geneva, Switzerland) (Entchev *et al.*, 2000); *UAS-RFP-Atg5* was kindly gifted by Katja

Koehler (Institute of Molecular Systems Biology, ETH Zurich) (Barth *et al.*, 2011); *UAS-Rheb* and *TSCQ87X* (*Tsc^{null}*) were kindly provided by Sean Oldham (Sanford-Burnham Medical Research Institute, La Jolla, CA) (Tapon *et al.*, 2001); *UAS-mCh-Zda* and *UAS-GFP-DFCP1* lines were generated by germline transformation.

Cloning and transgenic lines generation

Zonda locus was analyzed using FlyBase genome browser (www.flybase.org). Assembly

PCR was used to generate a fusion between the coding sequences of mCherry and Zda, with the following primers:

Zda Fw: CACCATGGATACGGAGAAGTCTAGCAGCAGC

Zda Rv: TTAGTACTTGTAAACGATAAATAGCCACGC

Zda -mCherry tail Fw: CTGTACAAGATGGATACGGAGAAGTC-TAGCAGCAGC

mCherry Fw: CACCATGGTGAGCAAGGGCGAGGAGGAT

Cherry Rv-Zda tail: CGTATCCATCTTGTACAGCTCGTCCATGC-CGCCGGT

The amplified fragments were subcloned into a pENTR/D-Topo plasmid and then transferred to a pUASg destination vector. Transgenic lines bearing the UAS-mCh-Zonda construct was generated by transposase-mediated genome integration (Spradling and Rubin, 1982).

UAS-GFP-DFCP1 was generated by cloning the GFP-DFCP1 sequence into pUAST from a previously described plasmid (Axe *et al.*, 2008), kindly provided by Nicholas Kistakis (University of Cambridge).

RT-PCR

Total RNA was isolated from embryos of the desired genotypes using the Trizol Reagent (Invitrogen). Genomic DNA was cleared out from RNA samples using the Ambion's DNA-free kit. cDNA was synthesized from 1–1.5 µg of RNA using oligo-dT as a primer and SuperScript III First-Strand Synthesis System (Invitrogen). RT-PCR was performed using Taq DNA polymerase (Invitrogen) and SYBR-Green and ROX (Invitrogen) as fluorescent dyes. Three independent biological samples were analyzed in each experiment. The following primers were used:

Zda Fw: GTACAGACGTGCCCTCGACTTTCT

Zda Rv: GTCAGTTCGAGAGCTCCAAGTCT

Tub Fw: ATCCCCAACACGTGAAGAC

Tub Rv: GCCTGAACATAGCGGTGAAC

Tissue staining, visualization, and image processing of *Drosophila* tissues

Third instar larvae were dissected in phosphate-buffered saline (PBS) and fixed in 4% formaldehyde (Sigma) for 2 h (fat body) at room temperature, washed three times in PBS-0.1% Triton X-100, and mounted in 40% glycerol for direct visualization of tissues. When needed, 300 nM 4',6-diamidino-2-phenylindole (DAPI) was added to the first washing step.

For LysoTracker staining, the reagent was added to unfixed tissues and directly visualized as previously described (Scott *et al.*, 2004). Tissues were imaged using a Zeiss confocal microscope LSM

710, using a 20× or 63× Zeiss Plan-Apochromat objective (NA 1.0 and 1.4, respectively) or a 40× Zeiss Plan-Neofluor objective (NA 1.3). When needed images were deconvoluted using Huygens Professional deconvolution software from Scientific Volume Imaging. Omegasome three-dimensional reconstructions were performed with Imaris software from Bitplane (Oxford Instruments), using confocal Z-stacks comprising up to 32 optical slices. For counting GFP-2xFYVE foci in Figure 3, a threshold was set using ImageJ to eliminate background signal. The cells were divided in two regions: a perinuclear region of 5 μm around the nuclei and a peripheral region in between the border of the cell and the perinuclear region (red and blue lines, respectively).

Transmission electron microscopy

Larvae were dissected and fixed overnight at 4°C using 2.5% glutaraldehyde in 0.1 M phosphate buffer, pH 7.4, followed by postfixation in 1% osmium tetroxide for 1 h. Samples were stained overnight at 4°C in 2% uranyl acetate and dehydrated with ethanol. Next, samples were embedded in Epoxy resin (Durcupan) and 60- to 70-nm sections were cut. Images were obtained using a transmission electron microscope (TEM-Zeiss-EM109T) and photographed on a Gatan ES1000W digital camera. A total of 20–30 12,000× magnification images were taken randomly from at least three animals per genotype, and the area of autophagic structures was manually encircled for area quantification with the ImageJ software.

Protein homogenates and Western blot analysis

Twenty larvae of the indicated genotype were homogenized in 200 μl of lysis buffer (50 mM HEPES, pH 7.4, 150 mM KCl, 6.5% glycerol, 0.5 mM dithiothreitol [DTT], 0.1% Triton X-100, and complete protease inhibitor tablet [Roche]). Samples were spun at 10,000 × g for 10 min at 4°C. Proteins were quantified in the supernatant using the bicinchoninic acid (BCA) method. Proteins (40 mg) were separated in 10% polyacrylamide gel and transferred to a nitrocellulose membrane. Membrane was blocked with 5% milk in TBS buffer with 0.1% Tween. Membranes were incubated overnight at 4°C with primary antibodies (anti-*Drosophila* phospho-S6K, cell signaling). Blots were incubated in goat anti-rabbit-HRP secondary antibody and diluted 1:30,000 in 3% milk/TBST (Tris buffered saline tween) for 1 h at room temperature. Blots were washed in TBST and then incubated with enhanced chemiluminescence (ECL) reagent (GE Healthcare), and signal was detected using ImageQuant LAS 4000 (GE Healthcare).

Cloning and construction of plasmids

Plasmids were made using the Gateway recombination system from Invitrogen. Full-length cDNA clone of Zonda was obtained from the DNASU plasmid repository, Arizona State University (Clone ID:DmCD00768948). Specific deletion mutations were generated by using QuickChange site-directed mutagenesis strategy (Stratagene, 200523). Full-length construct of DmVps34 was a kind gift from Tor Erik Rusten, Department of Molecular Cell Biology, Institute for Cancer Research, Oslo University Hospital, Norway. Vps34 cDNA was subcloned into a Gateway compatible entry vector by traditional restriction digestion-based cloning. All plasmids were verified by restriction digestions and DNA sequencing (BigDye Applied Biosystems, 4337455). Oligonucleotides used for mutagenesis and sequencing were obtained from Invitrogen.

Recombinant protein production and GST pull down

GST or GST tagged protein were expressed in *Escherichia coli* strain BL21 (DE3). GST or GST fusion proteins were purified and immobilized on glutathione-sepharose 4 Fast Flow beads (GE Healthcare,

17-5132-01). Myc-tagged proteins of interest were translated in vitro using TNT T7 coupled reticulocyte lysate system (Promega) in the presence of ³⁵S-labeled methionine. In vitro-translated proteins were preincubated with 10 μl of glutathione-sepharose beads with 100 μl of NETN buffer (50 mM Tris, pH 8.0, 150 mM NaCl, 1 mM EDTA, 0.5% Nonidet P-40) with cOmplete Mini EDTA-free protease inhibitor cocktail (1 tablet/10 ml) (11836170001; Roche Applied Science) for 30 min to reduce unspecific binding. Preincubated lysate was then incubated with the immobilized GST fusion protein for 2 h at 4°C. Beads were washed five times with NETN buffer, boiled with 2X SDS gel loading buffer (125 mM Tris, pH 6.8; 4% SDS, 0.04% bromophenol blue, 8% sucrose, 100 mM DTT), and subjected to SDS-PAGE. Gels were stained with Coomassie brilliant blue to visualize GST fusion proteins and vacuum dried. Signals from ³⁵S-labeled protein were detected using a Fujifilm bioimaging analyzer BAS-5000 (Fuji). Signals from ³⁵S-labeled protein were measured as units of photostimulated luminescence and quantitated relative to those obtained for 10% or 5% of the in vitro-translated lysate.

Statistical analysis

Unless indicated otherwise, statistical significance was calculated using one-way analysis of variance (ANOVA) followed by a Tuckey's test with a 95% confidence interval ($p < 0.05$). When needed Grubb's test was used to identify the values that were significant outliers from the rest ($p < 0.05$) (<https://graphpad.com/quickcalcs/grubbs2/>). Normality was tested with Shapiro Wilks' test and Q-QPlot. When needed, data were transformed to $\log(n+1)$ or to square root to reach normality. Homoscedasticity was tested with Bartlett's test. When necessary, the variances were modeled on VarIdent function using the smaller AIC criteria. Statistical analyses were executed using Rstudio, version 3.3.1. In all cases, error bars represent the SD. Each experiment was repeated at least three times. *N* indicates the number of cells or fields counted.

ACKNOWLEDGMENTS

We are grateful to Thomas Neufeld, Helmut Kramer, Tor Erik Rusten, Marcos Gonzalez-Gaitán, Katja Koehler, the Bloomington Stock Centre, and the Vienna *Drosophila* Resource Centre for fly strains and reagents. We thank all members of the Wappner and Colombo labs for discussions, Claudio Fader for his help with electron microscopy, Laura Ación for help with statistical analyses, Cristina Marino Buslje for help with bioinformatic analysis of Zda aminoacidic sequence, and Maximiliano Neme for help with confocal microscopy. This work was supported by Agencia Nacional de Promoción Científica y Tecnológica (ANPCyT) grants PICT 2011-2556 and PICT 2012-2376 to M.M.; PICT 2011-0090, PICT 2012-0214, and PICT 2014-0649 to P.W., and PICT 2008-0192 and PICT 2011-0455 to M.I.C. A.V. and R.V.R.-C. are doctoral fellows of ANPCyT, and M.M., M.O.A., E.S., M.I.C., and P.W. are career researchers of Consejo Nacional de Investigaciones Científicas y Técnicas (CONICET).

REFERENCES

- Albu S, Romanowski CP, Letizia Curzi M, Jakubcakova V, Flachskamm C, Gassen NC, Hartmann J, Schmidt MV, Schmidt U, Rein T, et al. (2014). Deficiency of FK506-binding protein (FKBP) 51 alters sleep architecture and recovery sleep responses to stress in mice. *J Sleep Res* 23, 176–185.
- Anding AL, Baehrecke EH (2015). Vps15 is required for stress induced and developmentally triggered autophagy and salivary gland protein secretion in *Drosophila*. *Cell Death Differ* 22, 457–464.
- Axe EL, Walker SA, Manifava M, Chandra P, Roderick HL, Habermann A, Griffiths G, Ktistakis NT (2008). Autophagosome formation from membrane compartments enriched in phosphatidylinositol 3-phosphate

- and dynamically connected to the endoplasmic reticulum. *J Cell Biol* 182, 685–701.
- Barth JM, Szabad J, Hafen E, Kohler K (2011). Autophagy in *Drosophila* ovaries is induced by starvation and is required for oogenesis. *Cell Death Differ* 18, 915–924.
- Barth S, Edlich F, Berchner-Pfannschmidt U, Gneuss S, Jahreis G, Hasgall PA, Fandrey J, Wenger RH, Camenisch G (2009). Hypoxia-inducible factor prolyl-4-hydroxylase PHD2 protein abundance depends on integral membrane anchoring of FKBP38. *J Biol Chem* 284, 23046–23058.
- Bhujabal Z, Birgisdottir AB, Sjøttem E, Brenne HB, Overvatn A, Habisov S, Kirkin V, Lamark T, Johansen T (2017). FKBP8 recruits LC3A to mediate Parkin-independent mitophagy. *EMBO Rep* 18, 947–961.
- Biazik J, Yla-Anttila P, Vihinen H, Jokitalo E, Eskelinen EL (2015). Ultrastructural relationship of the phagophore with surrounding organelles. *Autophagy* 11, 439–451.
- Bjorkoy G, Lamark T, Brech A, Outzen H, Perander M, Overvatn A, Stenmark H, Johansen T (2005). p62/SQSTM1 forms protein aggregates degraded by autophagy and has a protective effect on huntingtin-induced cell death. *J Cell Biol* 171, 603–614.
- Chang YY, Neufeld TP (2009). An Atg1/Atg13 complex with multiple roles in TOR-mediated autophagy regulation. *Mol Biol Cell* 20, 2004–2014.
- Chen Y, Klionsky DJ (2011). The regulation of autophagy—unanswered questions. *J Cell Sci* 124, 161–170.
- Entchev EV, Schwabedissen A, Gonzalez-Gaitan M (2000). Gradient formation of the TGF-beta homolog Dpp. *Cell* 103, 981–991.
- Eskelinen EL (2005). Maturation of autophagic vacuoles in mammalian cells. *Autophagy* 1, 1–10.
- Gillooly DJ, Morrow IC, Lindsay M, Gould R, Bryant NJ, Gaullier JM, Parton RG, Stenmark H (2000). Localization of phosphatidylinositol 3-phosphate in yeast and mammalian cells. *EMBO J* 19, 4577–4588.
- Gu W, Wan D, Qian Q, Yi B, He Z, Gu Y, Wang L, He S (2014). Ambra1 is an essential regulator of autophagy and apoptosis in SW620 cells: pro-survival role of Ambra1. *PLoS One* 9, e90151.
- Hara T, Mizushima N (2009). Role of ULK-FIP200 complex in mammalian autophagy: FIP200, a counterpart of yeast Atg17? *Autophagy* 5, 85–87.
- Itakura E, Mizushima N (2010). Characterization of autophagosome formation site by a hierarchical analysis of mammalian Atg proteins. *Autophagy* 6, 764–776.
- Juhász G, Hill JH, Yan Y, Sass M, Baehrecke EH, Backer JM, Neufeld TP (2008). The class III PI(3)K Vps34 promotes autophagy and endocytosis but not TOR signaling in *Drosophila*. *J Cell Biol* 181, 655–666.
- Juhász G, Puskas LG, Komonyi O, Erdi B, Maroy P, Neufeld TP, Sass M (2007). Gene expression profiling identifies FKBP39 as an inhibitor of autophagy in larval *Drosophila* fat body. *Cell Death Differ* 14, 1181–1190.
- Kamada Y, Yoshino K, Kondo C, Kawamata T, Oshiro N, Yonezawa K, Ohsumi Y (2010). Tor directly controls the Atg1 kinase complex to regulate autophagy. *Mol Cell Biol* 30, 1049–1058.
- Kang CB, Hong Y, Dhe-Paganon S, Yoon HS (2008). FKBP family proteins: immunophilins with versatile biological functions. *Neurosignals* 16, 318–325.
- Karanasios E, Ktistakis NT (2015). Live-cell imaging for the assessment of the dynamics of autophagosome formation: focus on early steps. *Methods* 75, 54–60.
- Kishi-Itakura C, Koyama-Honda I, Itakura E, Mizushima N (2014). Ultrastructural analysis of autophagosome organization using mammalian autophagy-deficient cells. *J Cell Sci* 127, 4089–4102.
- Laplante M, Sabatini DM (2009). mTOR signaling at a glance. *J Cell Sci* 122, 3589–3594.
- Lee SB, Kim S, Lee J, Park J, Lee G, Kim Y, Kim JM, Chung J (2007). ATG1, an autophagy regulator, inhibits cell growth by negatively regulating S6 kinase. *EMBO Rep* 8, 360–365.
- Lindmo K, Brech A, Finley KD, Gaumer S, Contamine D, Rusten TE, Stenmark H (2008). The PI 3-kinase regulator Vps15 is required for autophagic clearance of protein aggregates. *Autophagy* 4, 500–506.
- Lu Q, Yang P, Huang X, Hu W, Guo B, Wu F, Lin L, Kovacs AL, Yu L, Zhang H (2011). The WD40 repeat PtdIns(3)P-binding protein EPG-6 regulates progression of omegasomes to autophagosomes. *Dev Cell* 21, 343–357.
- Marquez RT, Xu L (2012). Bcl-2:Beclin 1 complex: multiple mechanisms regulating autophagy/apoptosis toggle switch. *Am J Cancer Res* 2, 214–221.
- Matsunaga K, Morita E, Saitoh T, Akira S, Ktistakis NT, Izumi T, Noda T, Yoshimori T (2010). Autophagy requires endoplasmic reticulum targeting of the PI3-kinase complex via Atg14L. *J Cell Biol* 190, 511–521.
- Mizushima N, Levine B, Cuervo AM, Klionsky DJ (2008). Autophagy fights disease through cellular self-digestion. *Nature* 451, 1069–1075.
- Newsome TP, Asling B, Dickson BJ (2000). Analysis of *Drosophila* photoreceptor axon guidance in eye-specific mosaics. *Development* 127, 851–860.
- Perrimon N, Gans M (1983). Clonal analysis of the tissue specificity of recessive female-sterile mutations of *Drosophila melanogaster* using a dominant female-sterile mutation *Fs(1)K1237*. *Dev Biol* 100, 365–373.
- Proikas-Cezanne T, Takacs Z, Donnes P, Kohlbacher O (2015). WIPI proteins: essential PtdIns3P effectors at the nascent autophagosome. *J Cell Sci* 128, 207–217.
- Pulipparacharuvil S, Akbar MA, Ray S, Sevrioukov EA, Haberman AS, Rohrer J, Kramer H (2005). *Drosophila* Vps16A is required for trafficking to lysosomes and biogenesis of pigment granules. *J Cell Sci* 118, 3663–3673.
- Roberts R, Ktistakis NT (2013). Omegasomes: PI3P platforms that manufacture autophagosomes. *Essays Biochem* 55, 17–27.
- Russell RC, Tian Y, Yuan H, Park HW, Chang YY, Kim J, Kim H, Neufeld TP, Dillin A, Guan KL (2013). ULK1 induces autophagy by phosphorylating Beclin-1 and activating VPS34 lipid kinase. *Nat Cell Biol* 15, 741–750.
- Saftig P, Klumperman J (2009). Lysosome biogenesis and lysosomal membrane proteins: trafficking meets function. *Nat Rev Mol Cell Biol* 10, 623–635.
- Sanchez-Wandelmer J, Ktistakis NT, Reggiori F (2015). ERES: sites for autophagosome biogenesis and maturation? *J Cell Sci* 128, 185–192.
- Scott RC, Juhász G, Neufeld TP (2007). Direct induction of autophagy by Atg1 inhibits cell growth and induces apoptotic cell death. *Curr Biol* 17, 1–11.
- Scott RC, Schuldiner O, Neufeld TP (2004). Role and regulation of starvation-induced autophagy in the *Drosophila* fat body. *Dev Cell* 7, 167–178.
- Shirane M, Nakayama KI (2003). Inherent calcineurin inhibitor FKBP38 targets Bcl-2 to mitochondria and inhibits apoptosis. *Nat Cell Biol* 5, 28–37.
- Shravage BV, Hill JH, Powers CM, Wu L, Baehrecke EH (2013). Atg6 is required for multiple vesicle trafficking pathways and hematopoiesis in *Drosophila*. *Development* 140, 1321–1329.
- Simonsen A, Tooze SA (2009). Coordination of membrane events during autophagy by multiple class III PI3-kinase complexes. *J Cell Biol* 186, 773–782.
- Spradling AC, Rubin GM (1982). Transposition of cloned P elements into *Drosophila* germ line chromosomes. *Science* 218, 341–347.
- Tapon N, Ito N, Dickson BJ, Treisman JE, Hariharan IK (2001). The *Drosophila* tuberous sclerosis complex gene homologs restrict cell growth and cell proliferation. *Cell* 105, 345–355.
- Wucherpfennig T, Wilsch-Brauninger M, Gonzalez-Gaitan M (2003). Role of *Drosophila* Rab5 during endosomal trafficking at the synapse and evoked neurotransmitter release. *J Cell Biol* 161, 609–624.
- Zhang J, Schulze KL, Hiesinger PR, Suyama K, Wang S, Fish M, Acar M, Hoskins RA, Bellen HJ, Scott MP (2007). Thirty-one flavors of *Drosophila* rab proteins. *Genetics* 176, 1307–1322.